Structural Changes and Reversibility Upon Deintercalation of Li from $LiCoPO_4$ Derivatives

J. G. Lapping[a], O. J. Borkiewicz[b], K. M. Wiaderek[b], J. L. Allen[c], T. R. Jow[c], J. Cabana[a]

[a]Department of Chemistry, University of Illinois at Chicago, Chicago, Illinois, 60607, United States of America

[b]Advanced Photon Source, Argonne National Laboratory, Lemont, Illinois 60439, United States

[c]U.S. Army Research Laboratory, Sensors and Electron Devices Directorate, 2800 Powder Mill Road, Adelphi, MD 20783, United States

Keywords: Lithium-ion battery, operando x-ray diffraction, lithium cobalt phosphate, crystallography, electrochemistry

Abstract

In an effort to improve the cycle life and rate capability of olivine $LiCoPO_4$, Cr, Fe, and Si were added to produce nominal $Li_{1.025}Co_{0.84}Fe_{0.10}Cr_{0.05}Si_{0.01}(PO_4)_{1.025}$. This cathode material has comparable energy density to $LiCoPO_4$, with markedly improved electrochemical performance. Here we apply *operando* X-ray diffraction to gain understanding of the unique crystallographic delithiation mechanism of this new substituted electrode material. Throughout charging, the extent of solid solution domains was significantly increased in $Li_{1.025}Co_{0.84}Fe_{0.10}Cr_{0.05}Si_{0.01}(PO_4)_{1.025}$ and $LiCo_{0.75}Fe_{0.25}PO_4$ compared to $LiCoPO_4$. These domains reduce mechanical strain during electrode function, providing a clear explanation for the high durability with Co substitution. $Li_{1.025}Co_{0.84}Fe_{0.10}Cr_{0.05}Si_{0.01}(PO_4)_{1.025}$ operated at notably higher average potential than $LiCo_{0.75}Fe_{0.25}PO_4$, which would increase the energy density of the cell. *Ex situ* measurements reveal the persistence of structural irreversibilities in the substituted phase after the first cycle, identifying avenues for further improvement in durability. This finding sheds light into strategies for judicious cation substitution in $LiCoPO_4$ electrodes to maximize cycle life while preserving high energy density, especially compared to $LiFePO_4$.

Introduction

In an effort to develop a rechargeable lithium-ion battery that can provide a functional alternative to fossil fuels, significant improvements need to be made to the storage capability of current commercial systems. For over twenty years, $LiFePO_4$ has been exhaustively researched for its commercial implementation as a cathode material, driven by its high stability, cycle life, and a moderate operating voltage (3.45V vs Li^+/Li).[1,2] In spite of its commercial success, it does not enable batteries that meet current goals in energy density for transportation, leading to the exploration of alternative olivine-structured lithium transition metal orthophosphates. In 2000, Amine *et al.* first reported $LiCoPO_4$,[3] which cycles reversibly at 4.8V vs Li^+/Li. By substituting Co for Fe, there is virtually no penalty in theoretical capacity (170 mAh/g for Fe compared to 167 mAh/g for Co) but an immediate theoretical energy density boost by almost 40% is attained. Unfortunately, compared to $LiFePO_4$, $LiCoPO_4$ suffers from poor cycle stability and rate performance, which is mainly ascribed to its low electronic conductivity[4] coupled to its propensity to defects that block transport.[5,6]

Learning from strategies that have improved the performance of $LiFePO_4$, ion substitution has been utilized as a strategy to overcome some of the inefficiencies of $LiCoPO_4$. By substituting Co for small quantities of other elements, the operating potential is not substantially lowered while carrier transport within the crystal structure is improved, delithiated states can be stabilized, and less reactive species can be formed at the electrode surface.[7-9] While Fe is the most common choice in the literature,[5] ion substitution in $LiCoPO_4$ has been shown to be more effective when Fe accompanied by other elements is used.[10-12] For instance, recently, utilizing a nominal stoichiometry of $Li_{1.025}Co_{0.84}Fe_{0.10}Cr_{0.05}Si_{0.01}(PO_4)_{1.025}$, a functional 1.2 Ah full cell was fabricated using a graphite anode.[10] Recent X-ray spectroscopic experiments have demonstrated the

beneficial effects of ion substitution on the electronic structure of $LiCoPO_4$. In particular, decreased deleterious surface reduction was found in delithiated states, stabilizing the interface with the electrolyte, while simultaneously demonstrating lower propensity to undergo evolution of oxygen and increased utilization of the $Co^{2+/3+}$ couple during electrochemical cycling.[12]

In addition to studies on the electronic structure of $LiCoPO_4$, the crystallographic changes that take place within the $LiCoPO_4$-$CoPO_4$ phase space have also been the subject of extensive studies.[13-16] Bramnik *et al*. first discovered that unsubstituted $LiCoPO_4$ undergoes electrochemical delithiation via two consecutive two-phase steps, forming a $Li_{2/3}CoPO_4$ structural intermediate.[17] Strobridge *et al.* further defined the local structure of $Li_{2/3}CoPO_4$ formed during electrochemical cycling using powder X-ray diffraction data coupled with solid-state NMR and first principles DFT calculations.[15] Recently, the variations in the delithiation mechanism with Co/Fe substitution has been explored in $LiCo_{1-x}Fe_xPO_4$. Strobridge *et al.* generally observed two intermediate phases when a substituted $LiFe_xCo_{1-x}PO_4$ electrode is delithiated. The first intermediate crystallographic phase corresponded to $Li_{2/3}Fe_xCo_{1-x}PO_4$ in all cases. The second intermediate phase arises after delithiation to form $Li_{1-x}(Fe^{3+})_x(Co^{2+})_{1-x}PO_4$, for $0<x<1$.[18] As such, the identity of the second crystallographic intermediate depends on the concentration of Fe within the electrode. Importantly, they also observed that for low concentrations of Fe ($0<x<0.5$), delithiation between $Li_{1-x}(Fe^{3+})_x(Co^{2+})_{1-x}PO_4$ and $Li_{2/3}CoPO_4$ occurs via a bulk single-phase delithiation mechanism, providing evidence that ion substitution can alter the delithiation mechanism. The reversibility of the reaction, especially vis-à-vis the coulombic efficiency of the cell, was not evaluated. Recently, *operando* XRD was measured for a cell containing $Li_{1.025}Co_{0.84}Fe_{0.10}Cr_{0.05}Si_{0.01}(PO_4)_{1.025}$ using a laboratory instrument.[10] While qualitative analysis suggested a similar crystallographic mechanism compared to unsubstituted $LiCoPO_4$, the analysis was hindered by the low intensity of

the measured peaks due to the small size of the crystallites in the electrode. This issue warranted further exploration using the high flux of synchrotron sources, which increase data quality by orders of magnitude, as demonstrated by Strobridge *et al.*[18]

In this work, we utilize synchrotron X-ray diffraction to shed light on the subtle crystallographic factors that contribute to the superior electrode properties of $Li_{1.025}Co_{0.84}Fe_{0.10}Cr_{0.05}Si_{0.01}(PO_4)_{1.025}$, using the unsubstituted compound and $LiFe_{0.25}Co_{0.75}PO_4$ as benchmarks. Even the small levels of substitution employed were sufficient to significantly extend compositional domains transforming through a solid solution mechanism. This mechanism typically leads to decreased localized gradients in strain within the electrode particles, providing an explanation to the extensive improvement in durability. Subsequent *ex situ* measurements of cycled electrodes revealed persistent sources of irreversibility even in $Li_{1.025}Co_{0.84}Fe_{0.10}Cr_{0.05}Si_{0.01}(PO_4)_{1.025}$, identifying avenues for further improvement of this material for application in Li-ion batteries with high energy density.

Methods

For all electrode materials, the starting materials, in addition to 5 wt% acetylene black based on expected final product mass, were ball milled for 90 min using a Spex SamplePrep 8000 M Mixer/Mill and a hardened steel grinding vial set. The milled powders were heated in a tube furnace at a rate of 10 $^{\circ}C\ min^{-1}$ to 700 $^{\circ}C$ under flowing N_2, held at 700 $^{\circ}C$ for 12 h and furnace cooled to room temperature. LiH_2PO_4, $Co(OH)_2$, $Si(OCOCH_3)_4$, Cr_2O_3 and $FeC_2O_4{\cdot}2H_2O$ were used as starting materials with mole ratios dependent on the desired product.

Operando diffraction experiments were performed utilizing pellet electrodes placed in the AMPIX[19] cell. Pellet electrodes totaling 25 mg were made by mixing 60 wt% electrode active

material, 20 wt% Vulcan carbon, and 20 wt% polytetrafluoro-ethylene (PTFE) (Sigma-Aldrich) using a mortar and pestle. The powder was pressed into a 13 mm pellet to 1.5 tons. The AMPIX cell was assembled in an argon-filled glovebox using Li metal as the counter electrode, with a 1M solution of $LiPF_6$ in a 1:1 mixture of ethylene carbonate/dimethyl carbonate (Tomiyama Pure Chemical Industries) and a microfiber filter as the separator. Cells were galvanostatically cycled at a rate of 0.1C.

The background contribution of the AMPIX cell was collected utilizing an AMPIX cell without a cathode. Detector position and angles were calibrated using a CeO_2 powder and GSAS II.[20] A Perkin-Elmer amorphous Si-based area detector measured the diffraction pattern with an X-ray wavelength of 0.2113 Å for 30 seconds per sample, at a distance of 95mm from the sample. Experiments were performed at beamline 11-ID-B at the Advanced Photon Source (APS), a synchrotron light source described in detail below.

High resolution synchrotron powder diffraction data were collected using beamline 11-BM at the Advanced Photon Source (APS), Argonne National Laboratory using an average wavelength of 0.4145 Å. Discrete detectors covering an angular range from -6 to 16 º 2θ were scanned over a 34º 2θ range, with data points collected every 0.001º 2θ and scan speed of 0.01º/s. Samples at the desired electrochemical states were produced by cycling conventional composite electrodes of $Li_{1.025}Co_{0.84}Fe_{0.10}Cr_{0.05}Si_{0.01}(PO_4)_{1.025}$ in coin cells using a Li metal counter electrode, as described in our previous report.[12]

Results

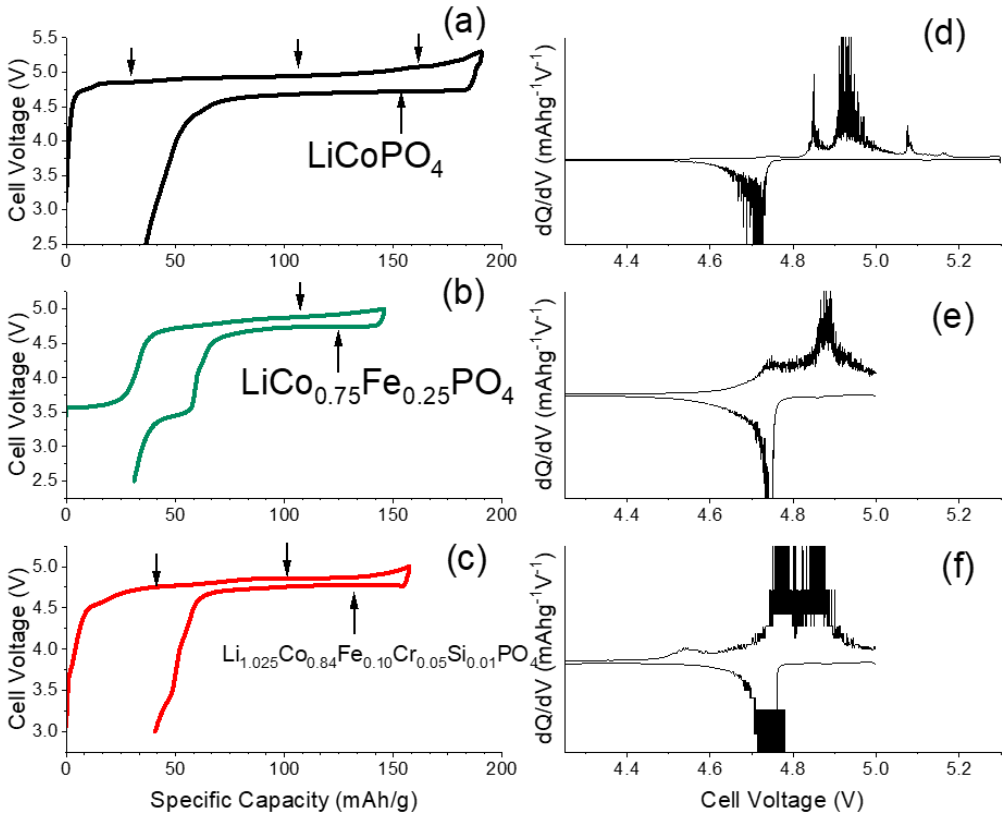

Figure 1. Electrochemical profiles of (a) $LiCoPO_4$, (b) $LiFe_{0.25}Co_{0.75}PO_4$, and (c) $Li_{1.025}Co_{0.84}Fe_{0.10}Cr_{0.05}Si_{0.01}(PO_4)_{1.025}$ collected during the first charge/discharge cycle within the AMPIX cell. Experiments were performed at a C/10 rate. The corresponding incremental capacity plots are also shown for (d) $LiCoPO_4$, (e) $LiFe_{0.25}Co_{0.75}PO_4$, and (f) $Li_{1.025}Co_{0.84}Fe_{0.10}Cr_{0.05}Si_{0.01}(PO_4)_{1.025}$. Arrows in galvanostatic cycling curves indicate cell potentials where peaks are observed in the incremental capacity plots.

The electrochemical profiles of pellet electrodes cycled in the AMPIX *operando* cell (**Figure 1)** were comparable to the profiles observed for thin film electrodes in coin cells.[12] During charging of $LiCoPO_4$ three plateaus are present; first at 4.84 V, corresponding to capacities between 16 and 39 mAh/g (0.095 – 0.23 mol Li deintercalated), second at 4.92 V, spanning between 54 and 140 mAh/g (0.32 – 0.84 mol Li), and third, at 5.1 V, between 159 and 168 mAh/g (0.95 – 1.00 mol Li); The plateau potentials were verified through incremental capacity plot (**Figure 1d**). The $LiCoPO_4$ electrode attained a final charge capacity of 188 mAh/g, 13% higher

than its theoretical capacity of 167 mAh/g (which correspond to 1.13 mol Li removed from $LiCoPO_4$). The extra capacity can be attributed to both electrolyte oxidation that occurs concurrently with deintercalation above 4.3 V and experimental error in active material mass estimation of the pellet electrode. $LiCoPO_4$ was the only electrode material in this study to be charged to 5.3 V vs Li (ion-substituted derivatives were charged to 5 V vs Li). A higher redox potential is needed for $LiCoPO_4$ in order to attain capacities commensurate with the ion-substituted electrode materials, consistent with the greater extent of cell polarization (**Figure 1d-f**), but a consequence of this is higher amounts of electrolyte decomposition. On discharge (reintercalation), there was a single plateau at 4.70 V at which most of the capacity was realized. The unsubstituted $LiCoPO_4$ electrode achieved 153 mAh/g (0.92 mol Li), 81% of the attained charge capacity. Overall, the results are in line with previous reports of $LiCoPO_4$ cycling behavior in a coin cell.[5,11,12]

The $LiFe_{0.25}Co_{0.75}PO_4$ electrode showed a characteristic plateau at 3.57 V between 0 and 22 mAh/g (0 to 0.14 mol Li removed, **Figure 1b**), followed by a sharp increase until 4.76 V (43 mAh/g, or 0.26 mol Li). The plateau at 3.57V is consistent with the process being driven by the formal Fe^{2+}/Fe^{3+} redox couple.[1] There was region with a small slope up to 4.83V (81 mAh/g, or 0.49 mol Li), followed by an additional pseudo-plateau at 4.92 V, spanning until 130 mAh/g (or 0.81 mol Li). Additional capacity attained after 4.92 V occurred again with a significant slope in potential, confirmed by the absence of peaks in the corresponding regions of the incremental capacity plot (**Figure 1e**). These findings were also consistent with previous literature.[12,18] Upon discharge, there were two plateaus at 4.75 V and 3.44 V corresponding to the processes up to 65 mAh/g (0.39 mol Li) and 100 mAh/g (0.60 mol Li), respectively. The final discharge capacity was 115 mAh/g (0.69 mol Li), 79% of the charge capacity.

The $Li_{1.025}Co_{0.84}Fe_{0.10}Cr_{0.05}Si_{0.01}(PO_4)_{1.025}$ electrode (**Figure 1c**) had a characteristic shoulder at 4.55 V, and was largely devoid of a plateau below 4 V that could be ascribed to the Fe^{2+}/Fe^{3+}, consistent with previous reports.[10-12] In contrast to $LiCoPO_4$, which has an extremely flat voltage profile, there was a sloping region between 36 mAh/g (0.22 mol Li) and 84 mAh/g (0.50 mol Li) centered around 4.75V. There was also a plateau between 85 mAh/g (0.51 mol Li) and 142 mAh/g (0.85 mol Li) at 4.9 V. The final charge capacity attained was 156 mAh/g, corresponding to 0.93 mol Li. On discharge, the largest plateau was observed at 4.76 V, attaining a capacity of 50 mAh/g, corresponding to 0.3 mol Li. There was an additional small plateau at 3.5 V. All remaining capacity was attained via a sloping voltage profile. A final discharge capacity of 116 mAh/g (0.69 mol Li) was achieved, corresponding to a 74.6% coulombic efficiency in the first cycle. Compared to cycling in a coin cell,[10-12] while a smaller value of charge and, especially, discharge capacity was observed overall, the general shape of the cycling curve was reproduced in an AMPIX cell. The difference in attained capacity can be partially be attributed to the electrode thickness, as pellet electrodes studied in the AMPIX cell were significantly thicker than electrodes cast on Al foil for cycling in coin cells (~18 vs. ~3 mg/cm^2, respectively). It is worthy of notice that the shape of the electrochemical profile above 4.5 V was subtly different on charge and discharge, suggesting the possibility of a different chemical pathway.

The diffraction profiles collected during the electrochemical cycling, plotted in the form of a contour plot of pattern number vs 2θ, with diffraction intensity as the color dimension are shown in **Figure 2**. Pattern numbers were separated temporally by 30 min per scan number. Miller indices for the most intense lines in the plots are provided in **Figure S1**. The galvanostatic cycling curves associated with each contour plot are shown in **Figure 2** as well, plotted as scan number vs cell voltage, for convenient comparison of charge state and diffraction pattern. A fundamental

challenge with this type of analysis lies in limits of angular resolution due to the short wavelength employed at the beamline. In the case of subtle structural changes with small variations in cell parameter, the angle of the new diffraction peaks could be too close to the original diffraction peak, introducing uncertainty in the assignment of a mechanism, especially in the existence of simultaneous peak broadening, as is the case here. For this reason, diffraction peaks at higher angles were visually inspected as well. **Figure 3** and **Figure 4** contain the change in (020) reflection as a function of scan number as a contour plot and stacked 1-D diffraction patterns, respectively, and **Figure 5** depicts the stacked diffraction peaks found between 7.9° and 8.5°, 2θ. The position of the (020) reflection was used as a proxy for the changes involved in phase transformation, because it is sensitive to the width of the unit cell. The region at high angle was chosen to maximize resolution, at the expense of a complex distribution of peaks (**Table S1** in the Supporting Information).

Both the contour maps and individually stacked diffraction patterns show differences in the charge/discharge mechanism for the three electrodes. For $LiCoPO_4$, (**Figure 3a**, **Figure 4a**, and **Figure 5a**), the (020) reflection, found at 4.08°, decreases in intensity to be replaced with a new reflection at 4.14° for an intermediate phase corresponding to $Li_{2/3}CoPO_4$, consistent with previous reports,[13,15,17] and a completely delithiated phase at approximately 4.18° in 2θ. In **Figure 5a**, during charging, it is immediately evident the initial reflections disappear without change in 2θ, being replaced by peaks at different angles, which also never shift. Because some of the reflections arise at lower angles than their initial counterparts, and others arise at higher angles, this demonstrates that the lattice parameters must be changing differently (i.e. expansion in one direction with contraction in a different one). The $LiCoPO_4$-$Li_{2/3}CoPO_4$ transition correlated well with the initial plateau at 4.84 V, with a total capacity corresponding to ~0.3 mol equivalents of Li

removed from the material (**Figures 3a, d**), indicating a faradaic efficiency of close to 100% at these potentials of operation. In contrast, it is worth noting that the formation of $CoPO_4$ was never complete, always co-existing with $Li_{2/3}CoPO_4$ at 4.14[o] (**Figure 4a)**. This observation confirms that, despite the high capacity measured in the cell, the electrode did not fully delithiate, as in our previous study with thinner electrodes in coin cells.[12] Therefore, the faradaic efficiency notably decreased as the potential was increased, especially beyond 5 V.

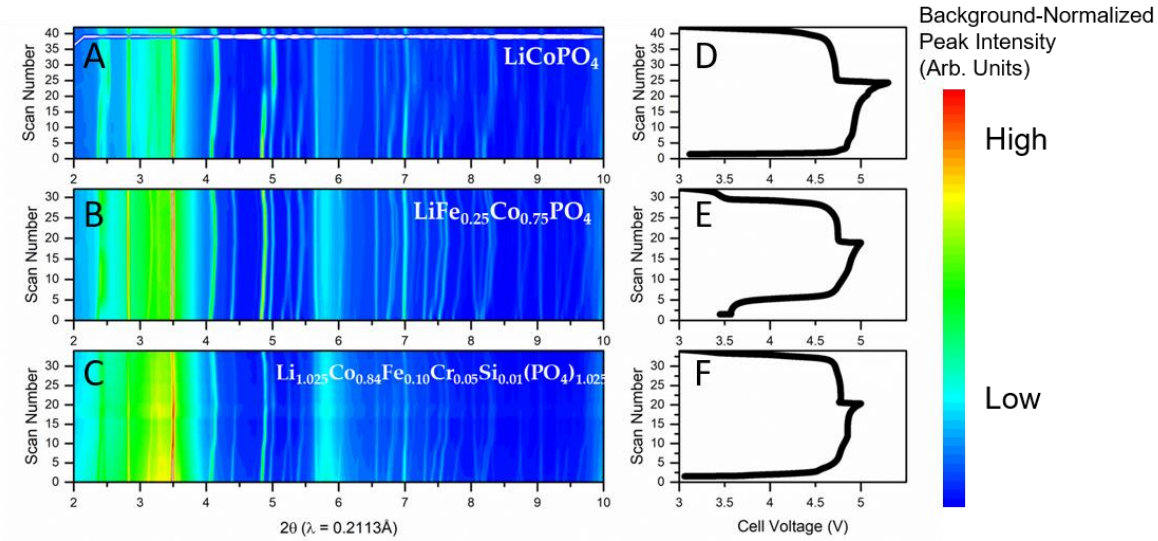

Figure 2. (a-c) Diffraction contour maps for (a) $LiCoPO_4$, (b) $LiFe_{0.25}Co_{0.75}PO_4$, and (c) $Li_{1.025}Co_{0.84}Fe_{0.10}Cr_{0.05}Si_{0.01}(PO_4)_{1.025}$ collected during the first charge/discharge cycle. (d-e) correlated galvanostatic (C/10) cycling curve for (d) $LiCoPO_4$, (e) $LiFe_{0.25}Co_{0.75}PO_4$, and (f) $Li_{1.025}Co_{0.84}Fe_{0.10}Cr_{0.05}Si_{0.01}(PO_4)_{1.025}$. The electrochemical profiles are the same as Figure 1. The white region in scan 37 in A corresponds to a brief period during which the synchrotron beam was down.

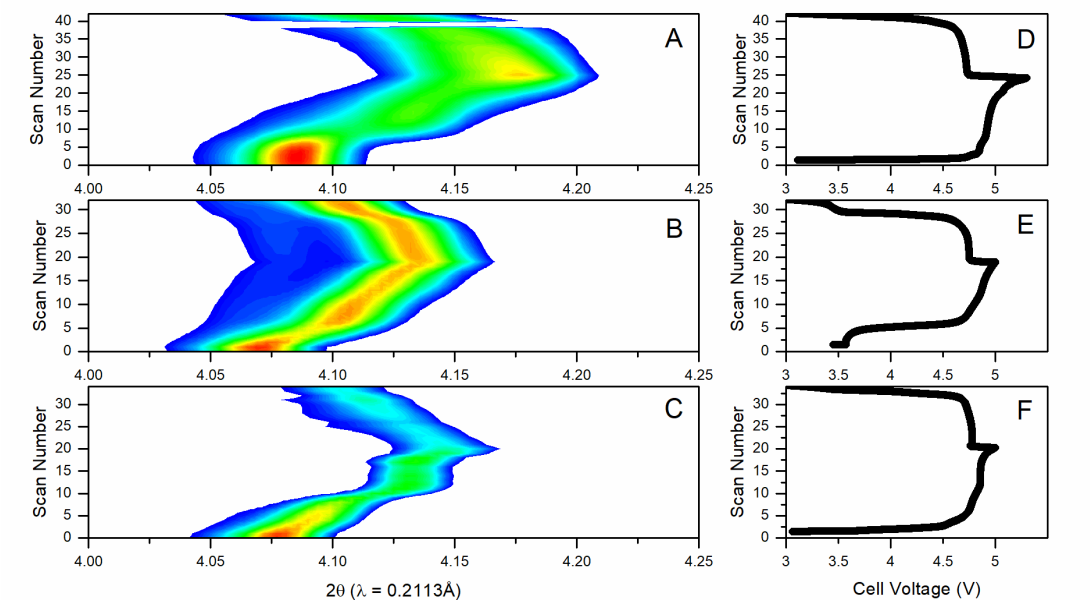

Figure 3. Contour map showing evolution of (020) reflection (left) and correlated galvanostatic (C/10) cycling curve (right) for first charge/discharge cycle for (a,d) $LiCoPO_4$, (b,e) $LiFe_{0.25}Co_{0.75}PO_4$, and (c,f) $Li_{1.025}Co_{0.84}Fe_{0.10}Cr_{0.05}Si_{0.01}(PO_4)_{1.025}$. The electrochemical profiles are the same as Figure 1. The gap in panel (a) corresponds to a brief period in which the synchrotron beam was turned off.

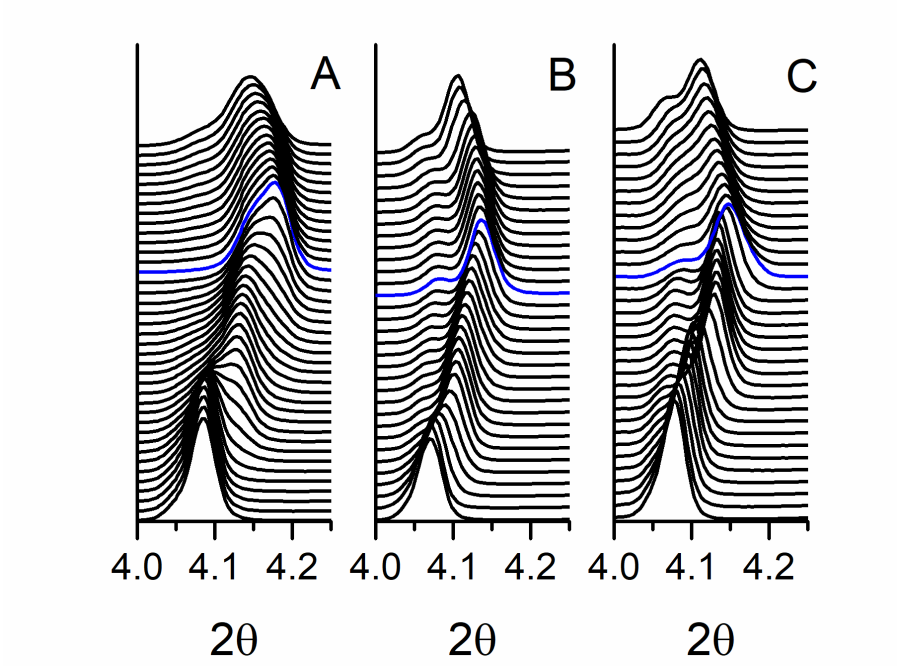

Figure 4. Diffraction patterns of (a) $LiCoPO_4$, (b) $LiFe_{0.25}Co_{0.75}PO_4$, and (c) $Li_{1.025}Co_{0.84}Fe_{0.10}Cr_{0.05}Si_{0.01}(PO_4)_{1.025}$ collected during the first charge/discharge cycle, featuring the (020) reflection. Scan number increases vertically, beginning with the pristine electrode material; the highlighted pattern in blue represents the switch from charge to discharge in all spectra.

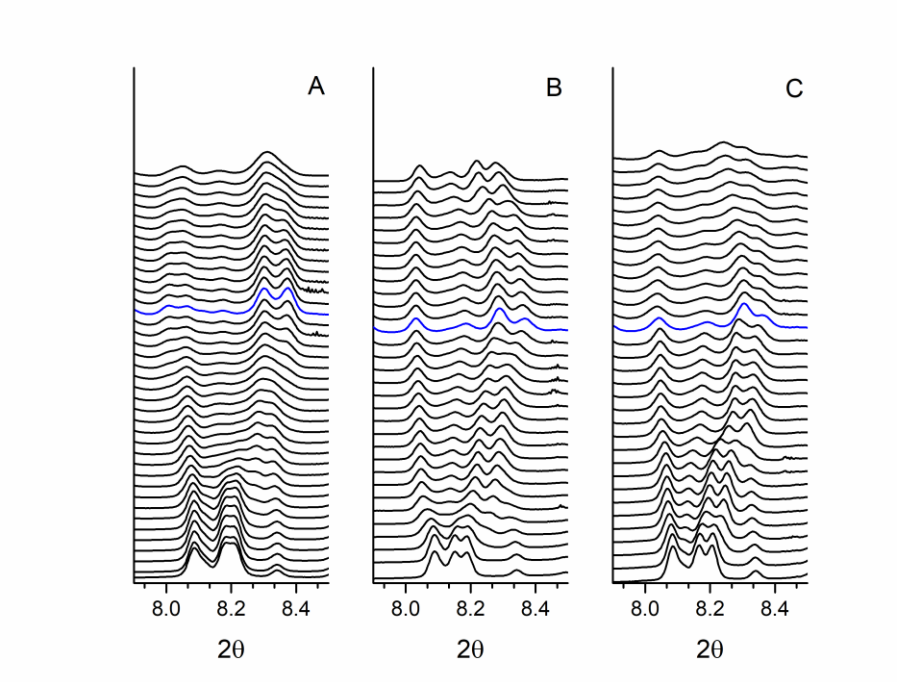

Figure 5. Diffraction patterns of for (a) $LiCoPO_4$, (b) $LiFe_{0.25}Co_{0.75}PO_4$, and (c) $Li_{1.025}Co_{0.84}Fe_{0.10}Cr_{0.05}Si_{0.01}(PO_4)_{1.025}$ collected during the first charge/discharge cycle, for reflections between 7.9° and 8.5° 2θ. Scan number increases vertically, beginning with the pristine electrode material; the highlighted pattern in blue represents the switch from charge to discharge in all spectra.

Subtle differences were observed on discharge. There was an overall increase in broadening of the peaks during cycling, likely due to strain associated with the presence of multiple crystallographic phases coexisting within a particle. Unfortunately, the broadening was within the limits of resolution of the beamline, complicating the analysis. First, only changes in the distribution of the underlying intensity of the diffraction peaks was observed in the early stages, as would be expected if the ratio of two overlapping, yet immobile sets of peaks changed. This process was followed by variations in the line shape of the peaks, such as the growth of a shoulder at 4.08° (**Figure 3a**, **Figure 4a**), and an overall trend at higher angles that was best explained by a two-phase behavior (**Figure 5a**). Lastly, it is worth noting that the (020) reflection never returned to the original angle in 2θ. This observation suggests the reaction was not completely reversed, explaining some of the capacity loss observed in the first cycle.

The first stages of the reaction of $LiFe_{0.25}Co_{0.75}PO_4$ appeared to be two-phase, leading approximately to $Li_{0.84}Fe_{0.25}Co_{0.75}PO_4$ (**Figure 3b**, **Figure 4b**, and **Figure 5b)**. This effect was visualized most clearly in **Figure 5b**, where the peak locations of $LiFe_{0.25}Co_{0.75}PO_4$ remained largely unchanged for the first three scans, aside from a change in the distribution of intensity, and then new diffraction peaks were clearly visible (see, for instance, the evolution of a complex line shape between 8.1° and 8.3° by the fourth scan). This behavior is the result of the emergence of a second phase at concentrations too low to be detected in the first few scans. A subsequent, substantial increase in broadening was also apparent. This effect has been previously ascribed to strain in the literature.[18] Further charging was accompanied by a clear, progressive shift of the peak positions, indicating a solid solution delithiation mechanism consistent with the sloping profile around 4.9 V. This observation differs from Strobridge *et al.*,[18] who reported a period in the *operando* experiment in which the shift of the peaks was temporarily paused, with no new reflections apparently emerging. Our observations suggest that the inherent mechanism of the material is solid solution in this compositional domain. We posit that the previous observations of invariance of peak positions at similar levels of delithiation were due to different electrode kinetics to this study, with particles completing their transformation discreetly in a highly asynchronous manner in different portions of the electrode, particularly with respect to X-ray illumination. On discharge, the peak shapes remained largely unchanged and, while a progressive shift was observed, their positions never completely returned to the original angles. This outcome again demonstrates incomplete relithiation, consistent with the coulombic inefficiency in the cycle.

The peaks of $Li_{1.025}Co_{0.84}Fe_{0.10}Cr_{0.05}Si_{0.01}(PO_4)_{1.025}$ smoothly shifted for the first 12 scans, indicative of a mechanism of solid solution consistent with the sloping voltage profile. (**Figure 3c**, **Figure 4c**, and **Figure 5c**) Strobridge *et al.* proposed that a phase of stoichiometry $Li_{1-x}Co_{1-}$

$_xFe_xPO_4$ forms via a two-phase step for all values of *x*.[18] In the case of 10% Fe substitution, this would occur during the first 10% of delithiation, which corresponds to the first two scans. Insufficient temporal resolution was attained during this experiment run, and, as such, this possibility should be the focus of further study. The solid-solution behavior is followed by a period during which, despite the fact that current was passing through the cell, there appeared to be no significant changes in peak locations, aside from a subtle change in relative intensity of the reflections between 8.25 and 8.4°. This period coincided with the sharp voltage plateau at 4.9 V (**Figure 1c**). It was followed by a sudden change in peak position in the last two patterns. In this case, this behavior was reminiscent of what Strobridge *et al.* reported for $LiFe_{0.125}Co_{0.875}PO_4$, which shows a similar level of Co substitution.[18] In contrast, Liu *et al.* observed a clear solid solution domain like in **Figures 3-5c** followed by a partial two-phase transition at the end of charge in laboratory *operando* XRD patterns of a similar material.[10] This observation could provide an explanation to the lack of peak movement observed in a portion of our data, especially considering that the positions of the peaks of the most delithiated phase reported by Liu *et al.* were not reached in our experiments. It is possible to hypothesize that, in all cases, the reaction was delayed in the region illuminated by the X-ray beam, being ultimately incomplete when the charge cutoff was reached. In our case, this hypothesis would be supported by the charge capacity being below the theoretical value. Furthermore, the sudden change in peak position in the last two patterns is accompanied by a subtle increase in width, which could be sufficient to mask the growth of a second phase.

During discharge, the delithiation mechanism of $Li_{1.025}Co_{0.84}Fe_{0.10}Cr_{0.05}Si_{0.01}(PO_4)_{1.025}$ was difficult to ascertain by analyzing the (020) reflection (**Figure 4c**). The reflection appeared to shift to a lower angle, but due to resolution limits it was not possible to confidently elucidate whether

the reflection was truly moving, or if a secondary phase was growing at a lower angle. At higher angles (**Figure 5c**) there appeared to be an increase in width of the diffraction peaks during the first four scans of relithiation, with no obvious change in positions. This trend was followed by a clear period of smooth shift of all reflections, but going beyond the position of the peaks of the intermediate observed on charge without a seeming two-phase behavior. As with the other two compounds, the reflections were not restored to their positions of pristine $Li_{1.025}Co_{0.84}Fe_{0.10}Cr_{0.05}Si_{0.01}(PO_4)_{1.025}$ after a full discharge.

To further examine the structural changes during timescales of the reaction where single phases were observed, analysis of the changes in the cell parameters was performed on the two ion-substituted electrodes (**Figure 6**). Because the dominant delithiation mechanism in $LiCoPO_4$ is two-phase, the cell parameters did not change as a function of delithiation, only the relative concentrations of each crystallographic phase (i.e., intensity of the corresponding reflections). As such, for the $LiCoPO_4$ electrode, calculated cell parameters are provided based on single phase Pawley refinements performed on scans 0, 16, and 26 for the Li_1, $Li_{2/3}$, and Li_0 phases respectively (**Table 1**). Scan numbers were chosen based on visual inspection of where the (020) reflection for the corresponding phases was the most intense. The lattice parameters calculated in **Table 1** all fell within 1% of previously reported literature values for $LiCoPO_4$.[17] During charging (delithiation), the a and b lattice parameters decreased in size, while the c parameter increased, also consistent with previous reports.[17,18]

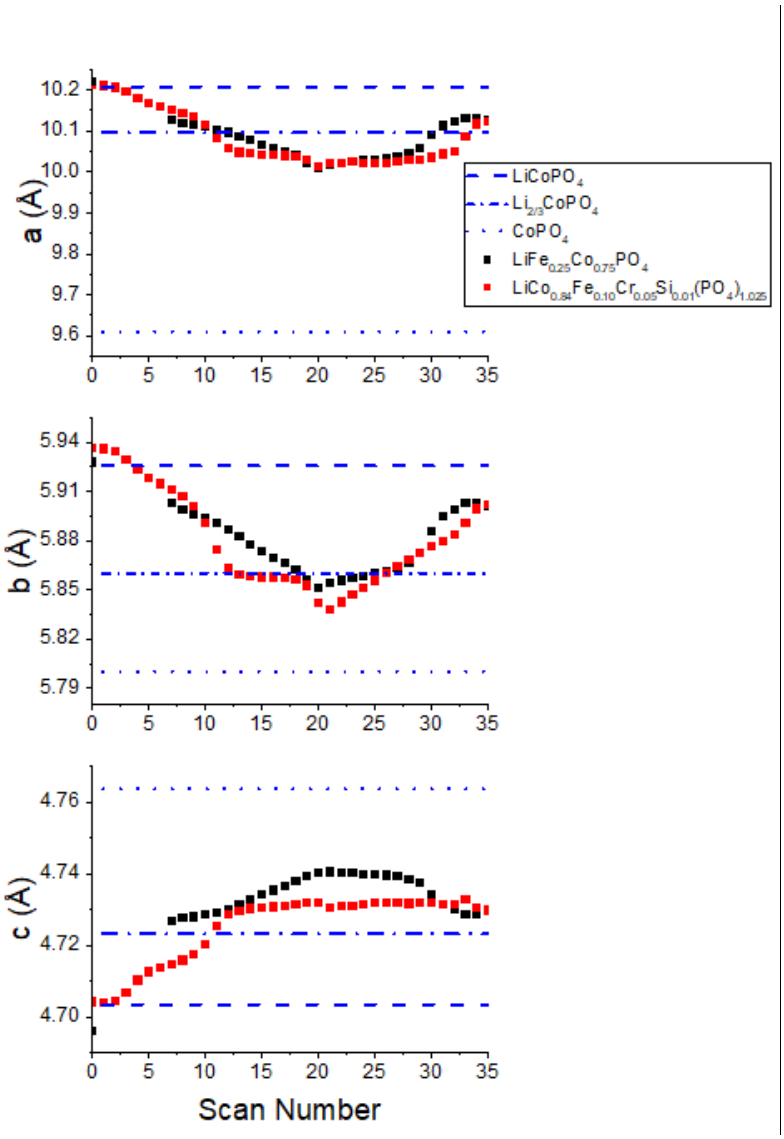

Figure 6. Evolution of cell parameters for $LiFe_{0.25}Co_{0.75}PO_4$ (black) and $Li_{1.025}Co_{0.84}Fe_{0.10}Cr_{0.05}Si_{0.01}(PO_4)_{1.025}$ (red) during the first charge/discharge cycle. Only the pristine state and values after scan 6 are shown for $LiFe_{0.25}Co_{0.75}PO_4$ because the transformation was 2-phase between scans 1 and 6, and, therefore, no change in cell parameter was observed. As a reference, the refined cell parameters for the fully lithiated, completely delithiated, and intermediate $LiCoPO_4$ phases are included in blue.

Table 1. Calculated cell parameters for Li_xCoPO_4, based on Pawley refinements of scans 0, 16, and 26, where the Li_1, $Li_{2/3}$, and Li_0 phases are most prevalent.

Composition	a (Å)	b (Å)	c (Å)
$LiCoPO_4$	10.21	5.93	4.70
$Li_{2/3}CoPO_4$	10.10	5.86	4.72

Li_0CoPO_4	9.61	5.80	4.76

According to the qualitative analysis above, the initial delithiation of $LiFe_{0.25}Co_{0.75}PO_4$ occurred through a 2-phase transformation. Therefore, following the same approach as $LiCoPO_4$, scans 1-6 are omitted, and the changes in cell parameter are monitored for this compound beginning in the pristine state and during the solid solution range. The goodness of the fits of the data was significantly better when these initial scans were omitted, validating the approach. The pristine cell parameters were close to unsubstituted $LiCoPO_4$, as expected from the similar ionic radius of Co^{2+} and Fe^{2+}.[21] During charging, the new partly delithiated phase (at scan 7) had lower a and b (10.13 and 5.90 Å), and higher c (4.73 Å) parameters than the pristine state. These parameters were similar to what was reported for the intermediate $Li_{0.75}Fe_{0.25}Co_{0.75}PO_4$ by Strobridge *et al.*,[18] consistent with the capacities accumulated at these potentials (**Figures 1b and 3b, e**). As the solid solution domain was reached, a and b decreased linearly to 10.01 and 5.85 Å, respectively. During this same interval, c increased from 4.73 to 4.74. The c parameter had a very slight increase in slope at scan 15. However, as a whole, the profile of the 25% Fe-substituted electrode was linear on charge, further supporting a delithiation mechanism of solid solution. It is possible that a second intermediate composition $Li_{2/3}Fe_{0.25}Co_{0.75}PO_4$ could have formed in the initial stages of this compositional window, but could not be resolved in this instrument due to the close proximity in cell parameters between the two intermediates, as observed by Strobridge *et al.*[18] The a and b cell parameters at the end of charge where higher than expected for $Fe_{0.25}Co_{0.75}PO_4$[18], whereas c was lower, revealing that delithiation was not complete in this electrode in the conditions of the *operando* measurement.

The changes in the XRD patterns of $Li_{1.025}Co_{0.84}Fe_{0.10}Cr_{0.05}Si_{0.01}(PO_4)_{1.025}$ could be satisfactorily accounted by a solid solution model with a near-perfect linear trend for scans 1-12 (nominal lithium content going down to ~0.4). Between these scans, a and b decreased from 10.22 and 5.94 to and 10.05 and 5.86, respectively. c increased from 4.70 to 4.73. It is worth considering the identity of this partially delithiated phase further. The process corresponds with the a relatively sloping region between 4.76 V and 4.83 V (**Figures 1c and 3c, f**), after which ~50% of total capacity of the electrode was accumulated. Indeed, the absolute value (84 mAh/g, see above) was equivalent to the extraction of ~0.5 mol Li. Therefore, while the cell parameters would be similar to the hypothetical $Li_{2/3}Co_{0.875}Fe_{0.125}PO_4$ phase proposed by Strobridge *et al.*,[18] coulometry strongly indicates that this phase actually contains a smaller amount of Li than postulated. This conclusion is supported by the fact that $Li_{2/3}CoPO_4$ was dominant approximately when only 1/3 of the capacity was accumulated in the $LiCoPO_4$ electrode, as discussed above, indicating that the faradaic efficiency was close to 100% at potentials below 4.85-4.90 V. Since both unsubstituted and substituted materials react at similar potentials, it is reasonable to assume similar faradaic efficiencies in all cases. It is also worthy of notice that Strobridge *et al.* systematically labeled intermediates as $Li_{2/3}Fe_xCo_{1-x}PO_4$ ($0.05 \leq x \leq 0.25$) even when these intermediates were detected at stages of the reaction with capacities significantly greater than 1/3 of the final value.[18] Furthermore, the volume of this $Li_{2/3}Fe_xCo_{1-x}PO_4$ intermediate did not significantly change with x, as would be expected from Vegard's law if the lithium content was constant. All in all, these observations suggest that the lithium content of this intermediate may also depend on the transition metal ratio in the M site of the olivine structure.

Between scans 13 and 19, there was only a minor change in cell parameters in the $Li_{1.025}Co_{0.84}Fe_{0.10}Cr_{0.05}Si_{0.01}(PO_4)_{1.025}$ electrode, consistent with aforementioned qualitative

observations of the diffraction patterns during this time interval. Assuming a faradaic efficiency of 100% for the process of deintercalation, this region would correspond to Li contents below 0.4 in the phosphate. Because current is indeed passing through the cell at this point, delithiation is either occurring via a two-phase mechanism, or only the electrolyte was electrochemically active, being oxidized at the electrode surface. The latter conclusion was rejected, however, because of: i) observed changes in XRD peak shapes that suggest the formation of secondary crystallographic phases, ii) the fact that the XRD peaks are not static at higher diffraction angles, and iii) the lack of such static behavior in the other two materials, which clearly react at very similar potentials. Indeed, the existence of concurrent consumption of current toward electrolyte decomposition at high potential is apparent for all compounds, since none displayed XRD patterns or reached cell parameters consistent with a pure Li_0 phase, in spite of the fact that, at least, close to 100% delithiation would be predicted from a coulometric standpoint. There is no clear reason not to expect that the associated faradaic inefficiencies were similar in all electrodes, given the similar compositions and potentials of operation. As already discussed above, this phenomenon is ascribed to the existence of a two-phase reaction where the delithiated phase formed primarily in domains that were not illuminated by the X-ray beam.

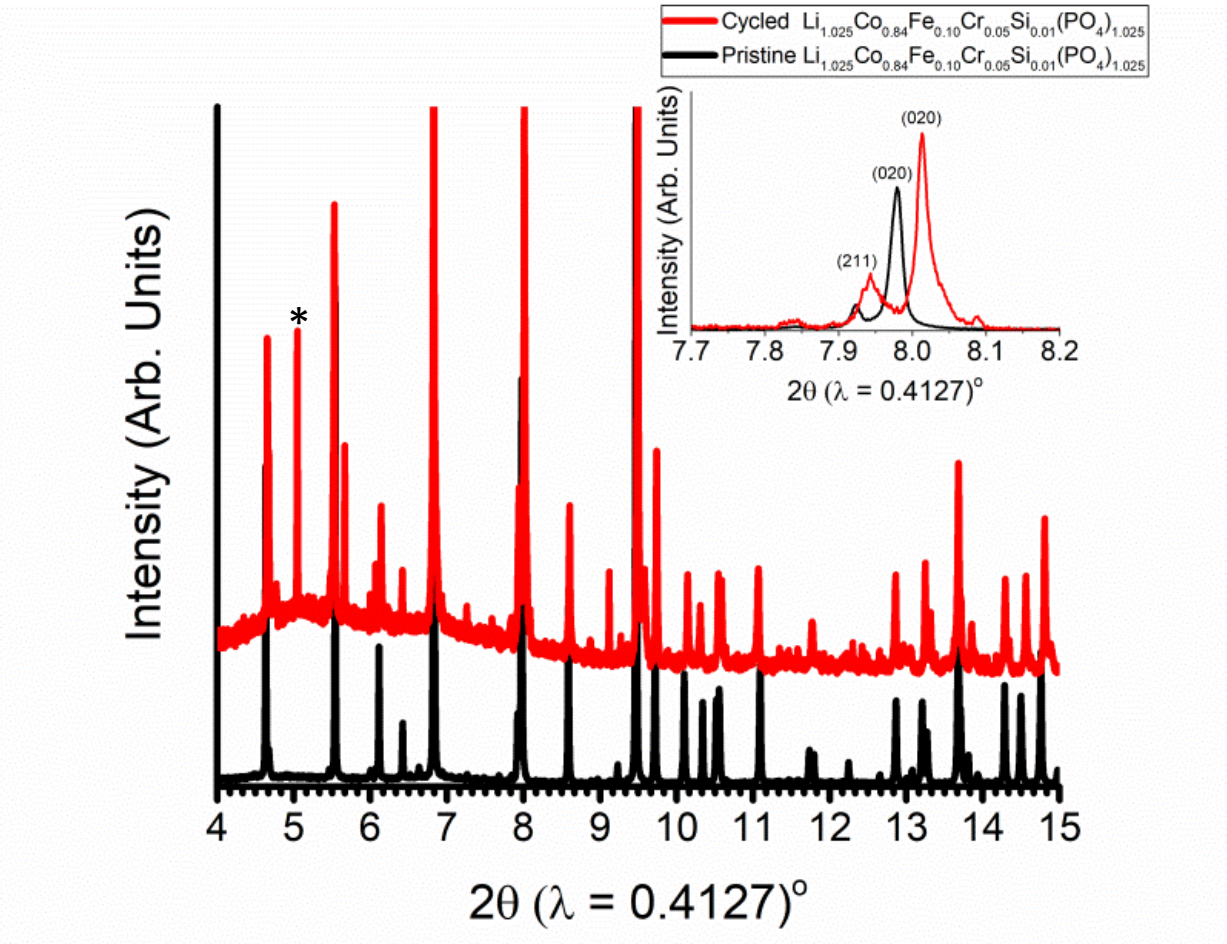

Figure 7. *Ex situ* high resolution XRD data, collected at beamline 11-BM at Argonne National Laboratory. Pristine $Li_{1.025}Co_{0.84}Fe_{0.10}Cr_{0.05}Si_{0.01}(PO_4)_{1.025}$ (black) and an electrode that has been charged to 5V then discharged to 2.5V (red).Data was normalized to the highest peak. "*" denotes the presence of an unidentified impurity in the *ex situ* sample. Inset between 7.7° and 8.2° to observe the evolution of the (020) reflection.

On discharge, the observed trends in cell parameter differ with what was observed during charging. For $LiFe_{0.25}Co_{0.75}PO_4$ and $Li_{1.025}Co_{0.84}Fe_{0.10}Cr_{0.05}Si_{0.01}(PO_4)_{1.025}$, the peaks showed a clear shift and no obvious decrease in the quality of the refinements was noted, supporting a mechanism of solid solution. However, the rate of change of all parameters increased between scans 21-30 and scans 30-35 in the $LiFe_{0.25}Co_{0.75}PO_4$ electrode, implying delithiation is occurring at a varying rate in the region illuminated by the X-rays, presumably compensated by the opposite trend in other regions of the electrode that were not observed. For

$Li_{1.025}Co_{0.84}Fe_{0.10}Cr_{0.05}Si_{0.01}(PO_4)_{1.025}$, the discharge profile was completely linear between scans 21-33, with a slight increase in rate of change for scans 34-35. This strongly suggests that while secondary crystallographic phases may form in this electrode material during charging, the mechanism appears dominated by solid solution character on discharge. The differing pathways are supported by the change in the electrochemical profile, which shows a single step with sloping potential on discharge, compared to multiple steps and one pronounced plateau on charge.

In terms of overall reversibility, no measured electrodes recovered their initial patterns and cell parameters. Ultimately, this is crystallographic evidence of capacity loss, consistent with the coulombic inefficiency of the cells in **Figure 1**. As discussed above, the high loading of the $Li_{1.025}Co_{0.84}Fe_{0.10}Cr_{0.05}Si_{0.01}(PO_4)_{1.025}$ electrodes used for operando measurements could be a factor in the inefficiency observed in our experiments. Since a greater discharge capacity was achieved in experiments with thinner electrodes in coin cells, the effect of cycling in those conditions was examined with high resolution *ex situ* synchrotron XRD (**Figure 7**). Visual comparison of the pattern of the electrode cycled in a coin cell with the pristine state confirms a persistent irreversibility despite the highly reversible capacity. New, sharp diffraction peaks were observed in the cycled electrode, e.g. at 5^{o}, which could not be indexed and were assigned to impurities from crystallization of electrolyte salts or products of oxidation, since they did not match any delitihiated phases. The cycled sample had calculated cell parameters of 10.17, 5.91, and 4.71 for a, b, and c, respectively. The calculated cell parameters for the cycled electrode are closer to the pristine state than the intermediate formulated as $Li_{0.5}Co_{0.84}Fe_{0.10}Cr_{0.05}Si_{0.01}(PO_4)_{1.025}$ above, indicating significant relithiation. In comparison, the cell parameters of the most discharged state measured in the AMPIX *operando* cell were 10.13, 5.90, and 4.73, respectively. Therefore, the final a and b

parameters are larger, and c is smaller in the sample cycled in the coin cell, corresponding to greater relithiation.

Taken together, these observations indicate that a persistent irreversibility exists for this material when cycled at C/10 even in fairly thin electrodes. The value of coulombic efficiency notably increases during subsequent cycles for all these electrode materials, indicating that reversibility increases upon cycling,[5,10,11] in a process that could be viewed as conditioning. Furthermore, Liu *et al.* reported almost complete restoration of the initial crystal structure when cycling at C/24,[10] suggesting that, while its performance clearly surpasses $LiCoPO_4$, $LiCo_{0.84}Fe_{0.10}Cr_{0.05}Si_{0.01}(PO_4)_{1.025}$ still suffers from kinetic limitations that reduce capacity even at moderate rates. Broadly speaking, there is still room for improving the rate capability of $LiCo_{0.84}Fe_{0.10}Cr_{0.05}Si_{0.01}(PO_4)_{1.025}$ through further judicious engineering of the electrodes to favor transport and thereby inch closer to the performance expectations of the final application.

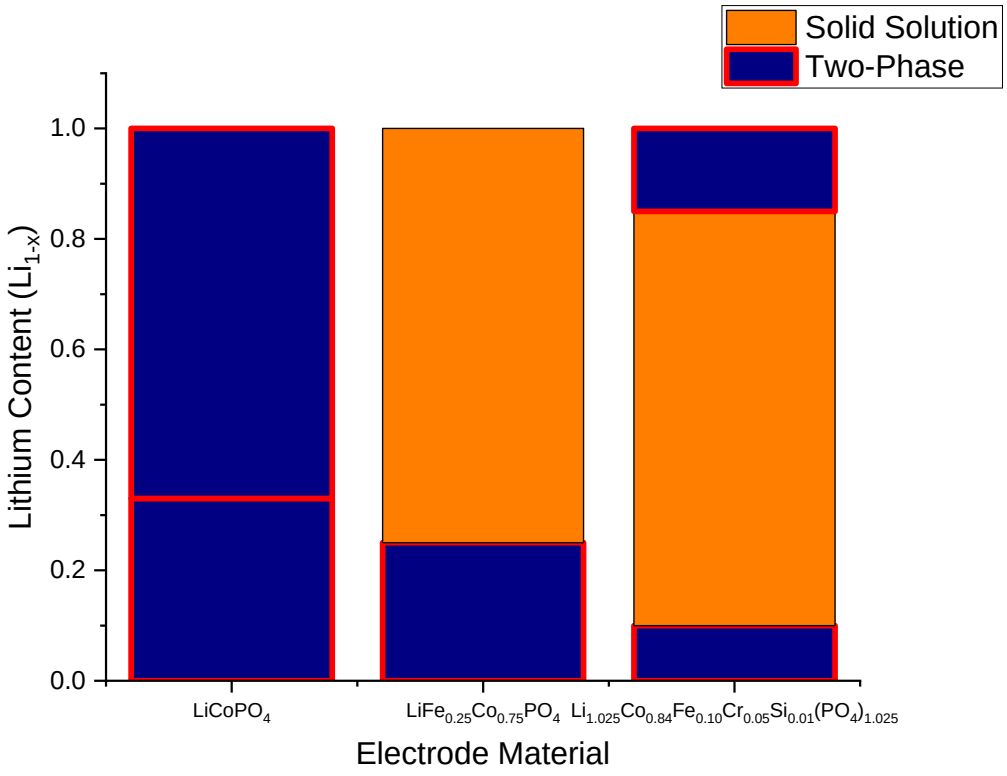

Figure 8. Summary of delithiation mechanisms observed in three $LiCoPO_4$-based electrodes during electrochemical charging.

Conclusion

The mechanism of reaction of three olivine type electrodes was studied by *operando* X-ray diffraction. $LiCoPO_4$, $LiFe_{0.25}Co_{0.75}PO_4$, and $Li_{1.025}Co_{0.84}Fe_{0.10}Cr_{0.05}Si_{0.01}(PO_4)_{1.025}$ all demonstrated unique electrochemical responses that were accompanied by unique delithiation mechanisms (**Figure 8**). Consistent with the literature, $LiCoPO_4$ was confirmed to follow two steps with a two-phase mechanism, with an intermediate of chemical formula approximately $Li_{2/3}CoPO_4$. The $LiFe_{0.25}Co_{0.75}PO_4$ electrode exhibited a two-phase delithiation mechanism followed by a solid-solution process after approximately 25% of the lithium had been extracted. Lastly, the patterns of the $Li_{1.025}Co_{0.84}Fe_{0.10}Cr_{0.05}Si_{0.01}(PO_4)_{1.025}$ electrode were well-modeled by a single phase delithiation mechanism up to 50% delithiation, but the trend at higher levels of

delithiation indicated the existence of two-phase behavior. Upon discharge, the mechanism was found to be more consistent with a further increase in the solid solution domains for both substituted materials, consistent with their asymmetric electrochemical profiles. Compared to $LiCoPO_4$, the fact that delithiation proceeds through significant regions of solid solution upon cation substitution helps to explain the superior performance of $Li_{1.025}Co_{0.84}Fe_{0.10}Cr_{0.05}Si_{0.01}(PO_4)_{1.025}$ in previous work. Solid solution domains will alleviate the mechanical stress associated with sudden changes in unit cell volume, which can lead to slower kinetics and even fracture, especially if the particles are not very small. However, *ex situ* analysis also revealed that even this optimized material still suffers from some irreversibility in the first cycle at moderate rate, offering an avenue for further incremental advances by tweaking electrode design. It is noteworthy that $Li_{1.025}Co_{0.84}Fe_{0.10}Cr_{0.05}Si_{0.01}(PO_4)_{1.025}$ performs at a higher average voltage than $LiFe_{0.25}Co_{0.75}PO_4$ due to the low concentration of Fe, which increases the energy density of the final Li-ion battery. Subsequent studies are needed to evaluate how the crystallographic delithiation mechanism is altered by changes in C-rate. These findings suggest that a rather unexplored pathway still exists for $LiCoPO_4$-based electrodes with high capacity and long cycle life, which could create a robust alternative to technology based on layered oxides.

Acknowledgements

Research was sponsored by the Army Research Laboratory and was accomplished under Cooperative Agreement Number W911NF-15-2-0010. The views and conclusions contained in this document are those of the authors and should not be interpreted as representing the official policies, either expressed or implied, of the Army Research Laboratory or the U.S. Government.

The U.S. Government is authorized to reproduce and distribute reprints for Government purposes notwithstanding any copyright notation herein. This research used resources of the Advanced Photon Source, a U.S. Department of Energy (DOE) Office of Science User Facility operated for the DOE Office of Science by Argonne National Laboratory under Contract No. DE-AC02-06CH11357.

Supporting Information. Miller indices of diffraction reflections measured and diffraction pattern of $LiCoPO_4$ with select Miller indices labelled.

Author Information:

Corresponding Author – Jordi Cabana – *Department of Chemistry, University of Illinois at Chicago, Chicago, Illinois, 60607, United States; Email:* jcabana@uic.edu

References

(1) Padhi, A. K. Phospho-olivines as Positive-Electrode Materials for Rechargeable Lithium Batteries. *J. Electrochem. Soc.* **1997,** *144* (4), 1188.

(2) Wang, J. J.; Sun, X. L. Olivine $LiFePO_4$: The Remaining Challenges for Future Energy Storage. *Energy Environ. Sci.* **2015,** *8* (4), 1110.

(3) Amine, K.; Yasuda, H.; Yamachi, M. Olivine $LiCoPO_4$ as 4.8 V Electrode Material for Lithium Batteries. *Electrochem. Solid-State Lett.* **2000,** *3* (4), 178.

(4) Zhang, M.; Garcia-Araez, N.; Hector, A. L. Understanding and Development of Olivine $LiCoPO_4$ Cathode Materials for Lithium-Ion Batteries. *J. Mater. Chem. A* **2018,** *6* (30), 14483.

(5) Allen, J. L.; Jow, T. R.; Wolfenstine, J. Improved Cycle Life of Fe-Substituted $LiCoPO_4$. *J. Power Sources* **2011,** *196* (20), 8656.

(6) Truong, Q. D.; Devaraju, M. K.; Tomai, T.; Honma, I. Direct Observation of Antisite Defects in $LiCoPO_4$ Cathode Materials by Annular Dark- and Bright-Field Electron Microscopy. *ACS Appl. Mater. Interfaces* **2013,** *5* (20), 9926.

(7) Chiang, C.-Y.; Su, H.-C.; Wu, P.-J.; Liu, H.-J.; Hu, C.-W.; Sharma, N.; Peterson, V. K.; Hsieh, H.-W.; Lin, Y.-F.; Chou, W.-C.; Lee, C.-H.; Lee, J.-F.; Shew, B.-Y. Vanadium Substitution of LiFePO4 Cathode Materials To Enhance the Capacity of $LiFePO_4$-Based Lithium-Ion Batteries. J. Phys. Chem. C 2012, 116, 24424−24429.

(8) Meethong, N.; Kao, Y.-H.; Speakman, S. A.; Chiang, Y.-M. Aliovalent Substitutions in Olivine Lithium Iron Phosphate and Impact on Structure and Properties. *Adv. Funct. Mater.* **2009,** *19* (7), 1060.

(9) Omenya, F.; Chernova, N. A.; Zhang, R.; Fang, J.; Huang, Y.; Cohen, F.; Dobrzynski, N.; Senanayake, S.; Xu, W.; Whittingham, M. S. Why Substitution Enhances the Reactivity of $LiFePO_4$. *Chem. Mater.* **2013,** *25* (1), 85.

(10) Liu, D.; Zhu, W.; Kim, C.; Cho, M.; Guerfi, A.; Delp, S. A.; Allen, J. L.; Jow, T. R.; Zaghib, K. High-Energy Lithium-Ion Battery using substituted $LiCoPO_4$: From coin type to 1 Ah cell. *J. Power Sources* **2018,** *388*, 52.

(11) Allen, J. L.; Allen, J. L.; Thompson, T.; Delp, S. A.; Wolfenstine, J.; Jow, T. R. Cr and Si Substituted-$LiCo_{0.9}Fe_{0.1}PO_4$: Structure, Full and Half Li-ion Cell Performance. *J. Power Sources* **2016,** *327*, 229.

(12) Lapping, J. G.; Delp, S. A.; Allen, J. L.; Allen, J. L.; Freeland, J. W.; Johannes, M. D.; Hu, L. H.; Tran, D. T.; Jow, T. R.; Cabana, J. Changes in Electronic Structure upon Li Deintercalation from $LiCoPO_4$ Derivatives. *Chem. Mater.* **2018,** *30* (6), 1898.

(13) Ehrenberg, H.; Bramnik, N. N.; Senyshyn, A.; Fuess, H. Crystal and Magnetic Structures of Electrochemically Delithiated $Li_{1-x}CoPO_4$ Phases. *Solid State Sci.* **2009,** *11* (1), 18.

(14) Kaus, M.; Issac, I.; Heinzmann, R.; Doyle, S.; Mangold, S.; Hahn, H.; Chakravadhanula, V. S. K.; Kubel, C.; Ehrenberg, H.; Indris, S. Electrochemical Delithiation/Relithiation of $LiCoPO_4$: A Two-Step Reaction Mechanism Investigated by *in Situ* X-Ray Diffraction, *in Situ* X-Ray Absorption Spectroscopy, and *ex Situ* $^7Li/^{31}P$ NMR Spectroscopy. *J. Phys. Chem. C* **2014,** *118* (31), 17279.

(15) Strobridge, F. C.; Clement, R. J.; Leskes, M.; Middlemiss, D. S.; Borkiewicz, O. J.; Wiaderek, K. M.; Chapman, K. W.; Chupas, P. J.; Grey, C. P. Identifying the Structure of the Intermediate, $Li_{2/3}CoPO_4$, Formed During Electrochemical Cycling of $LiCoPO_4$. *Chem. Mater.* **2014,** *26* (21), 6193.

(16) Nakayama, M.; Goto, S.; Uchimoto, Y.; Wakihara, M.; Kitajima, Y.; Miyanaga, T.; Watanabe, I. X-Ray Absorption Spectroscopic Study on the Electronic Structure of $Li_{1-x}CoPO_4$ electrodes as 4.8 V Positive Electrodes for Rechargeable Lithium Ion Batteries. *J. Phys. Chem. B* **2005,** *109* (22), 11197.

(17) Bramnik, N. N.; Nikolowski, K.; Baehtz, C.; Bramnik, K. G.; Ehrenberg, H. Phase Transitions Occurring Upon Lithium Insertion−Extraction of $LiCoPO_4$. *Chem. Mater.* **2007,** *19* (4), 908.

(18) Strobridge, F. C.; Liu, H.; Leskes, M.; Borkiewicz, O. J.; Wiaderek, K. M.; Chupas, P. J.; Chapman, K. W.; Grey, C. P. Unraveling the Complex Delithiation Mechanisms of Olivine-Type Cathode Materials, $LiFe_xCo_{1-x}PO_4$. *Chem. Mater.* **2016,** *28* (11), 3676.

(19) Borkiewicz, O. J.; Shyam, B.; Wiaderek, K. M.; Kurtz, C.; Chupas, P. J.; Chapman, K. W. The AMPIX Electrochemical Cell: a Versatile Apparatus for *in Situ* X-Ray Scattering and Spectroscopic Measurements. *J. Appl. Cryst.* **2012,** *45* (6), 1261.

(20) Toby, B. H.; Von Dreele, R. B. GSAS-II: the Genesis of a Modern Open-Source All Purpose Crystallography Software Package. *J. Appl. Cryst.* **2013,** *46* (2), 544.

(21) Shannon, R. D. Revised Effective Ionic Radii and Systematic Studies of Interatomic Distances in Halides and Chalcogenides. *Acta Cryst. A* **1976,** *32* (5), 751.

Table of Contents